significant, and showed no trend with dielectric constant. Thus, it appears that solvent effects are not important in those cases in which there are no changes in rotamer populations.[45]

Conclusions

Good correlations of the orthobenzylic coupling constants in methyl aromatic compounds and unsaturated compounds (having vinylic methyl groups) are found with the π-bond order η, the square of η, and the mutual atom–atom polarizability $\pi_{pp'}$. However, the linear dependence on η (which has no theoretical basis) gives values which are much too high in the region of very low bond orders.

In the extension of the study to molecules in which both conformational and bond order effects are important to the J_{ob}, it is found that the generalization of the relationship of coupling constant to $\pi_{pp'}$ to include angular factors gives results which are in very good agreement with the experimental results. The agreement is an improvement on the results based on the IND-O–FPT method[34] and is much better than the correlation with η^2. It seems likely that the inadequacy of the latter is due to the overestimation of J^σ.

The experimental and theoretical results presented here provide an important method for obtaining useful structural information in complex molecules.

Acknowledgment. This work was supported by Australian Research Grants Committee, Grant C7415407.

Registry No. 1, 108-88-3; **2**, 115-07-1; **3**, 91-57-6; **4**, 575-41-7; **5**, 581-42-0; **6**, 571-61-9; **7**, 84944-65-0; **8**, 613-26-3; **9**, 782-23-0; **10**, 1576-67-6; **11**, 1576-69-8; **12**, 7372-87-4; **13**, 33982-92-2; **14**, 90-12-0; **15**, 613-12-7; **16**, 883-20-5; **17**, 2871-91-2; **18**, 1705-84-6; **19**, 652-04-0; **20**, 2381-34-2; **21**, 2319-96-2; **22**, 3442-78-2; **23**, 3353-12-6; **24**, 1705-85-7; **25**, 13119-86-3; **26**, 3727-31-9; **27**, 96-39-9; **28**, 767-60-2; **29** (M = H), 768-49-0; **30**, 504-60-9; **31**, 452-68-6; **32**, 14495-51-3; **33** (R = CN), 16955-23-0; **33** (R = COOMe), 84944-66-1; **33** (R = NH_2), 16955-25-2; **33** (R = $NMe_3^+I^-$), 16955-26-3; **33** (R = Cl), 16954-29-3; **33** (R = OH), 2876-02-0; **34**, 99-99-0; **35**, 618-85-9; **36**, 119-33-5; **37a**, 58802-07-6; **37b**, 13771-37-4; **37c**, 13771-38-5; **38**, 84944-67-2; **39**, 33982-90-0; **40**, 84944-68-3; **41**, 13030-26-7; **42a**, 84944-69-4; **42b**, 84944-70-7; **43a**, 84944-71-8; **43b**, 84944-72-9; **43c**, 84944-73-0; **43d**, 84944-74-1; **44a**, 496-16-2; **44b**, 76429-69-1; **44c**, 84944-75-2; **44d**, 17403-47-3; **44e**, 17403-48-4; **44f**, 84944-76-3; **44g**, 84944-77-4; **45a**, 84944-78-5; **45b**, 86-73-7; **45c**, 7012-16-0; **45d**, 58775-05-6; **46**, 85026-14-8; **47**, 15656-90-3; **49** (X = H), 10239-86-8; **49** (X = CH_3), 84959-62-6; **49** (X = $CH(CO_2CH_3)_2$), 84944-79-6; **49** (X = C_6H_5), 84944-80-9; **49** (X = NH_2), 84944-81-0; **49** (X = Br), 84944-82-1; **49** (X = Cl), 84944-83-2; **49** (X = OH), 84944-84-3; **49** (X = $OCOCH_3$), 84944-85-4; **50** (X = H), 4208-97-3; **50** (X = CH_3), 84944-86-5; **50** (X = $CH(CO_2CH_3)_2$), 84944-87-6; **50** (X = C_6H_5), 84944-88-7; **50** (X = NH_2), 84944-89-8; **50** (X = Br), 29094-68-6; **50** (X = Cl), 84944-90-1; **50** (X = OH), 84944-91-2; **50** (X = $OCOCH_3$), 84944-92-3.

Supplementary Material Available: Data concerned with general experimental procedures, synthesis of compounds, and spectral analyses (112 pages). Ordering information is given on any current masthead page.

Mechanism of CO_2 Elimination from Ionized Methyl Haloacetates in the Gas Phase. Formation of $CH_3XCH_2^+\cdot$ and $CH_3XCHX^+\cdot$ (X = Cl, Br) Halonium Radical Ions

Yitzhak Apeloig,*[1a] Bernhard Ciommer,[1b] Gernot Frenking,[1b] Miriam Karni,[1a] Asher Mandelbaum,*[1a] Helmut Schwarz,*[1b] and Adrian Weisz[1a]

Contribution from the Department of Chemistry, Technion—Israel Institute of Technology, Haifa, Israel, and the Institut für Organische Chemie der Technischen Universität Berlin, D-1000 Berlin 12, West Germany. *Received March 31, 1982*

Abstract: The molecular ions of the methyl esters of chloro-, bromo-, dichloro-, and dibromoacetic acids undergo unimolecular elimination of CO_2 in the gas phase. Collisional activation (CA) mass spectrometry suggests that the resulting $[M - CO_2]^+\cdot$ ions possess novel types of hypervalent structures, i.e., $CH_3XCH_2^+\cdot$ and $CH_3XCHX^+\cdot$ (X = Cl, Br). MNDO and ab initio calculations show that the methylmethylenechloronium radical ion $CH_3ClCH_2^+\cdot$ and the isomeric chloroethane cation radical $CH_3CH_2Cl^+\cdot$ exist in a potential minimum. MNDO predicts that $CH_3ClCH_2^+\cdot$ is more stable than $CH_3CH_2Cl^+\cdot$ by 10.1 kcal mol^{-1}, whereas according to 6-31G* and UMP2/6-31G* $CH_3CH_2Cl^+\cdot$ is more stable by 9.1 and 6.4 kcal mol^{-1}, respectively. Several possible mechanisms for the dissociative rearrangement $ClCH_2COOCH_3^+\cdot \rightarrow CO_2 + CH_3ClCH_2^+\cdot$ were investigated computationally by MNDO. Selected intermediates and transition states were also calculated at the 4-31G level. Three competing processes for the unimolecular loss of CO_2 from ionized methyl chloroacetate are examined in detail. According to the calculations the energetically most favorable pathway for the formation of $CH_3ClCH_2^+\cdot$ from $ClCH_2COOCH_3^+\cdot$ commences with the migration of the ester methyl group to chlorine, followed by the elimination of CO_2 (i.e., $ClCH_2COOCH_3^+\cdot \rightarrow H_3CClCH_2COO^+\cdot \rightarrow CO_2 + CH_3ClCH_2^+\cdot$).

The study of simple molecules in the gas phase often provides an opportunity to generate species that, due to intermolecular reactions, cannot be observed in the condensed phase.[2] This holds in particular for ions, and it is the study of the "isolated" species (e.g., in the gas phase) that allows one to reveal their inherent properties and to study the mechanisms according to which the ions are generated.[3] We shall describe here the results of our combined experimental and theoretical investigation on the electron impact induced CO_2 loss from methyl haloacetates.

(1) (a) Technion Haifa. (b) Technische Universität Berlin.

(2) The case of the 2-adamantyl cation can be taken as a typical example. The only adamantyl cation detected so far in solution is the 1-adamantyl cation; there is no experimental indication for the existence of 2-adamantyl cation despite a substantial barrier (>30 kcal mol^{-1}) for the isomerization 2-adamantyl → 1-adamantyl cation. In the gas phase, however, both species were recently generated as stable cations and their inherent properties studies. See: (a) Wesdemiotis, C.; Schilling, M.; Schwarz, H. *Angew. Chem., Int. Ed. Engl.* **1979**, *18*, 950. (b) Houriet, R.; Schwarz, H. *Ibid.* **1979**, *18* 951.

(3) For leading references, see: (a) Williams, D. H. *Acc. Chem. Res.* **1977**, *10*, 280. (b) Bowen, R. D.; Williams, D. H.; Schwarz, H. *Angew, Chem., Int. Ed. Engl.* **1979**, *18*, 451. (c) Arnett, E. M. *Acc. Chem. Res.* **1973**, *6*, 404. (d) Kebarle, P.; Davidson, W. R.; Sunner, J.; Meza-Hajer, S. *Pure Appl. Chem.* **1979**, *51*, 63. (e) Levsen, K. "Fundamental Aspects of Organic Mass Spectrometry"; Verlag Chemie: Weinheim/Bergstrasse, Germany, 1978. (f) Bowers, M. T., Ed. "Gas Phase Ion Chemistry"; Academic Press: New York, 1979.

0002-7863/83/1505-2186$01.50/0

Table I. Collisional Activation Mass Spectra of $C_2H_5Cl^{+\cdot}$ and $C_2H_2D_3Cl^{+\cdot}$ Ions (m/z 64 and 67, Respectively) Formed from Several Precursors[a]

fragment ions, m/z	$CH_3CH_2Cl^{+\cdot}$ (6)	$1^{+\cdot} \rightarrow C_2H_5Cl^{+\cdot} + CO_2$	$CD_3CH_2Cl^{+\cdot}$ (6a)	$CH_2ClCO_2CD_3^{+\cdot} \xrightarrow{-CO_2}$ 1a $C_2H_2D_3^{+\cdot}$
66			34	9.6
65			8.2	2.4
64			4.1	1.1
63	38	9.3	3.9	4.9
62	8.9	2.6	1.7	4.5
61	5.7	11		
60	1.7	1.5		
54				1.4
53				14
51		2.1	1.3	10
50		12	2.6	1.7
49	63[b]	172[b]	40[b]	249[b]
48	9.7	31	7.7	25
47	7.4	20	5.9	15
33			5.2	2.8
32			50[b]	22[b]
31			20[b]	4.2[b]
30	4.8	2.7	52[b]	9.3[b]
29	36[b]	19[b]	14	4.6
28	55[b]	9.7[b]	6.9	2.0
27	19	6.4	4.3	0.9
26	4.9	2.3		

[a] The spectra were recorded with use of the "linked B/E scan" technique.[6] The relative abundances are given in percent and are normalized to $\Sigma_{\text{fragments}} = 100\%$. [b] Excluded from the normalization procedure are these fragment ions, which are also formed unimolecularly and whose relative intensity may be dependent upon the energy distribution function.[5]

The most abundant fragment ion formed from the molecular ion of methyl iodoacetate ($3^{+\cdot}$, eq 1) appears at m/z 73, corresponding to the loss of an iodine radical. In the 70-eV mass spectra of methyl chloro- and bromoacetates (**1** and **2**) the m/z 73 ion is practically absent. Instead, the spectra of the latter two esters exhibit prominent peaks at m/z 66 and 64 (relative abundance (RA) 6% and 22%) for $1^{+\cdot}$ and at m/z 110 and 108 (RA 15% and 15%) for $2^{+\cdot}$. According to high-resolution measurements these peaks arise from loss of CO_2 from the molecular ions.[4] A corresponding $[M - CO_2]^{+\cdot}$ ion was not observed in the mass spectrum of $3^{+\cdot}$. However, CO_2 elimination was also found to occur from the molecular ions of methyl dichloro- and dibromoacetates (**4** and **5**), giving rise to the formation of abundant

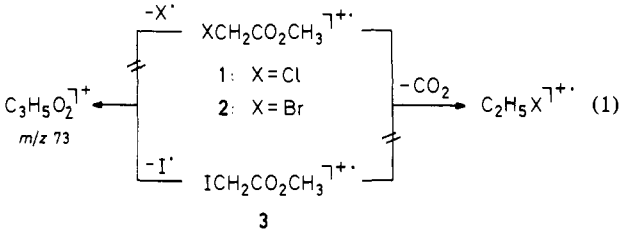

3

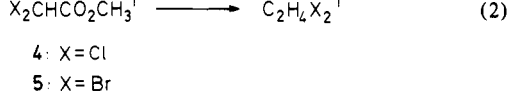

$C_2H_4X_2^{+\cdot}$ ions (X = Cl, 11%; X = Br, 16%). The subject of the present study is to determine the structure of the $[M - CO_2]^{+\cdot}$ ions and to elucidate the mechanism of their formation.

Structure of $[M - CO_2]^{+\cdot}$ Ions. The natural starting point for the elucidation of a reaction mechanism is to determine the structure of the products. For gaseous ions valuable structural information can be provided by collisional activation (CA) mass spectrometry,[5] as this method has proved to be reliable in determining the number and structures of ionic species existing in significant minima on the potential-energy surface. Consequently the CA spectra (for details see Experimental Section) of the $C_2H_5X^{+\cdot}$ (X = Cl, Br) ions obtained after CO_2 elimination from $1^{+\cdot}$ and $2^{+\cdot}$ were recorded and compared with the CA spectra of the $C_2H_5X^{+\cdot}$ ions generated by electron impact ionization of chloro- and bromoethane (**6** and **7**, eq 3). The spectral data, listed

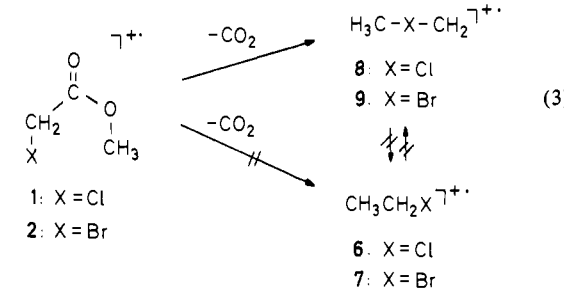

in Tables I and II, are significantly different for the $C_2H_5X^{+\cdot}$ ions, clearly indicating that the $[M - CO_2]^{+\cdot}$ fragments have structures that are different from those of the molecular ions of the corresponding haloethanes **6** and **7**. On the basis of the CA mass spectra, we suggest that the $[M - CO_2]^{+\cdot}$ ions, generated from **1** and **2**, have the methylmethylenehalonium radical structures **8** and **9**, which do not isomerize to the isomeric haloethane radical ions, **6** and **7**, on the time scale of the mass spectrometer ($t \geq 10^{-5}$

(4) The 70-eV mass spectra of **1** and **2** appear in EPA/NIH "Mass Spectral Data Base"; Heller, S. R., Milne, G. W. A., Eds.; U. S. Department of Commerce, National Bureau of Standards, 1978. The relative abundances extracted from these spectra are as follows: m/z 64, ~40% (for $1^{+\cdot}$); m/z 108, ~40% (for $2^{+\cdot}$). A note on the electron impact induced CO_2 loss from halogenated acetates has recently been published by Hesse and co-workers (Lorenzi-Riatsch, A.; Bild, N.; Hesse, M. *Helv. Chim. Acta* **1981**, *64*, 1563). These authors arrive at the very same conclusions as we do with regard to the structure of the $[M - CO_2]^{+\cdot}$ ions and the mechanism of their formations. But their intuitively derived structure assignment is supported neither by experimental facts nor by computational results. We should like to thank Prof. Hesse, Universität Zürich, for helpful correspondence on this subject.

(5) For reviews see: (a) Levsen, K.; Schwarz, H. *Angew. Chem., Int. Ed. Engl.* **1976**, *15*, 509. (b) McLafferty, F. W. "Chemical Applications of High Performance Mass Spectrometry"; American Chemical Society: Washington, D.C., 1978. (c) "Collision Spectroscopy"; Cooks, R. G., Ed.; Plenum Press: New York, 1978. (d) McLafferty, F. W. *Phil. Trans. R. Soc. London* **1979**, *293A*, 93. (e) Reference 3b,e.

(6) For details see: (a) Boyd, R. K.; Beynon, J. H. *Org. Mass Spectrom.* **1977**, *12*, 163. (b) Bruins, A. P.; Jennings, K. R.; Evans, S. *Int. J. Mass. Spectrom. Ion Phys.* **1978**, *26*, 395. (c) Schwarz, H.; Höhne, G.; Blender, J. M.; Veith, H. J. *VIA, Varian Instrum. Appl.* **1979**, *40*, 1.

Table II. Collisional Activation Mass Spectra of $C_2H_5Br^{+\cdot}$ (m/z 108) and $C_2H_2D_3Br^{+\cdot}$ (m/z 111)[a]

fragment ions, m/z	$CH_3CH_2Br^{+\cdot}$ (7)	$2^{+\cdot} \rightarrow C_2H_5Br^{+\cdot} + CO_2$	$CD_3CH_2Br^{+\cdot}$ (7a)	$CH_2BrCO_2CD_3^{+\cdot} \xrightarrow{-CO_2}$ 2a $C_2H_2D_3Br^{+\cdot}$
110			3.9	
109			3.9	
108			1.4	
107	20		1.1	1.9
106	2.2		0.9	2.0
105	2.4	4.4		
104	0.8			
98				2.2
97				30
95		6.3	3.0	11
94	1.6	31	2.5	2.6
93	40[b]	150[b]	29[b]	81[b]
92	11	27	8.7	23
91	13	19	11	17
81	6.4	2.2	9.4	2.3
80	6.6	1.9	4.6	
79	23	3.3	26	2.6
33			8.2	2.2
32			67[b]	31[b]
31			4.6	0.7
30	1.6	0.4	6.0[b]	1.6[b]
29	52[b]	21[b]	7.6	2.1
28	3.1	1.1	3.4	0.5
27	7.2	3.0		
26	1.0	0.4		

[a] See footnote *a* of Table I. [b] See footnote *b* of Table I.

s). The data in Table I provide valuable support for the structures **8** and **9**. Previous work[7] has shown that the collision-induced loss of CH_2 can be taken as evidence for the presence of a terminal methylene group. As can be seen from the data in Table I, CH_2 loss is an important process for the $[M - CO_2]^{+\cdot}$ ions formed from **1** or **2**. In contrast, collision-induced loss of CH_2 from the haloethanes **6** and **7** is either totally absent (**6**) or insignificant (**7**). Studies of the D-labeled isotopomers show that the process involves the original methylene group and is not preceded by hydrogen scrambling. In addition, the loss of a methyl radical under the condition of collisional activation is much more pronounced in the CA spectra of ions **8** and **9** in comparison to the haloethanes **6** and **7**. This is a direct consequence of the bonding properties of **8** and **9**, which will be discussed later. Moreover, the m/z 79 ion (Br^+) is of higher abundance in the CA spectra of $CH_3CH_2Br^{+\cdot}$ (**7**) and CD_3CH_2Br (**7a**) and much less pronounced in the spectra of the fragment ions generated via CO_2 loss from ionized **2** and **2a**.

A similar conclusion can be drawn for the structures of the $C_2H_4X_2^{+\cdot}$ ions generated by CO_2 loss from the dihaloacetates **4** and **5** (eq 4). The collisional activation spectra for these fragment

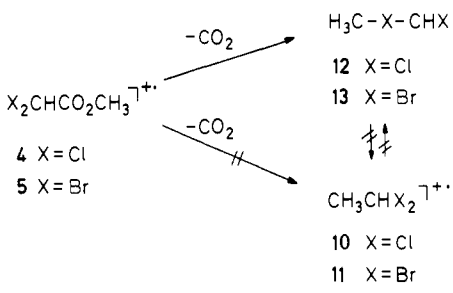

(4)

ions (shown in Table III) are again entirely different from the CA spectra obtained for the corresponding 1,1-dihaloethanes **10** and **11**. Here the striking differences of the m/z 27 ($C_2H_3^+$) ions on the one hand and the fragments caused by collision-induced losses of $CH_3\cdot$ and X· (X = Cl, Br) on the other hand can be used for the structure assignments. The $C_2H_3^+$ ion is of much higher abundance in the CA spectra of the dihaloethanes **10** and **11** than in those of the $[M - CO_2]^{+\cdot}$ ions. This behavior is in agreement with the structures of the molecular ions of **10** and **11**. Similarly, the substantially increased loss of X· from **10** and **11** compared with the $[M - CO_2]^{+\cdot}$ ions is easily explained. Loss of X· from **10** and **11** is expected to give rise to a closed-shell secondary cation stabilized by the remaining halo substituents, a process that for structural reasons is less likely to occur in the $[M - CO_2]^{+\cdot}$ ions.

(7) For other examples of diagnostically useful CH_2 losses upon collisional activation see: (a) Bowen, R. D.; Williams, D. H.; Schwarz, H.; Wesdemiotis, C. *J. Am. Chem. Soc.* **1979**, *101*, 4681. (b) Schwarz, H.; Wesdemiotis, C.; Levsen, K.; Bowen, R. D.; Williams, D. H. *Z. Naturforsch. B, Anorg. Chem., Org. Chem., Biochem., Biol.* **1979**, *34B*, 488. (c) Wesdemiotis, C.; Wolfschütz, R.; Höhne, G.; Schwarz, H. *Org. Mass Spectrom.* **1979**, *14*, 231. (d) Franke, W.; Schwarz, H.; Stahl, D. *J. Org. Chem.* **1980**, *45*, 3493. (e) Bowers, M. T.; Shuying, L.; Kemper, P.; Stradling, R.; Webb, H.; Aue, D. H.; Gilbert, J. R.; Jennings, K. R. *J. Am. Chem. Soc.* **1980**, *102*, 4830. (f) Apeloig, Y.; Franke, W.; Rappoport, Z.; Schwarz, H.; Stahl, D. *Ibid.* **1981**, *103*, 2770. (g) Schwarz, H.; Wesdemiotis, C.; Levsen, K.; Heimbach, H.; Wagner, W. *Org. Mass Spectrom.* **1979**, *14*, 244. (h) Hommes, H.; Terlouw, J. K. *Ibid.* **1979**, *14*, 51. (i) McLafferty, F. W.; Winkler, J. *J. Am. Chem. Soc.* **1974**, *96*, 5182. (j) Van de Graaf, B.; Dymerski, P. P.; McLafferty, F. W. *J. Chem. Soc., Chem. Commun.* **1975**, 978. (k) Levsen, K.; Schwarz, H. *J. Chem. Soc., Perkin Trans. 2* **1976**, 1231. (l) Köppel, C.; Van de Sande, C. C.; Nibbering, N. M. M.; Nishishita, T.; McLafferty, F. W. *J. Am. Chem. Soc.* **1977**, *99*, 2883. (m) Schwarz, H.; Wesdemiotis, C.; Heimbach, H.; Levsen, K. *Org. Mass Spectrom.* **1977**, *12*, 213. (n) Levsen, K.; Heimbach, H.; Van de Sande, C. C.; Monstrey, J. *Tetrahedron* **1977**, *33*, 1785. (o) Van de Graaf, B.; McLafferty, F. W. *J. Am. Chem. Soc.* **1977**, *99*, 6806, 6810. (p) Monstrey, J.; Van de Sande, C. C.; Levsen, K.; Heimbach, H.; Borchers, F. *J. Chem. Soc., Chem. Commun.* **1978**, 796. (q) Schwarz, H.; Williams, D. H.; Wesdemiotis, C. *J. Am. Chem. Soc.* **1978**, *100*, 7052. (r) Schwarz, H.; Wesdemiotis, C. *Org. Mass Spectrom.* **1979**, *14*, 25. (s) Schwarz, H.; Franke, W.; Chandrasekhar, J.; Schleyer, P. v. R. *Tetrahedron* **1979**, *35*, 1969. (t) Bowen, R. D.; Chandrasekhar, J.; Frenking, G.; Schleyer, P. v. R.; Schwarz, H.; Wesdemiotis, C.; Williams, D. H. *Chem. Ber.* **1980**, *113*, 1084. (u) Hemberger, P. H.; Kleingeld, J. C.; Levsen, K.; Mainzer, N.; Mandelbaum, A.; Nibbering, N. M. M.; Schwarz, H.; Weber, R.; Weisz, A.; Wesdemiotis, C. *J. Am. Chem. Soc.* **1980**, *102*, 3736. (v) Wagner, W.; Levsen, K.; Lifshitz, C. *Org. Mass Spectrom.* **1980**, *15*, 271. (w) Wesdemiotis, C.; Schwarz, H.; Budzikiewicz, H.; Vogel, E. *Ibid.* **1981**, *16*, 89. (x) Vajda, J. H.; Harrison, A. G.; Hirota, A.; McLafferty, F. W. *J. Am. Chem. Soc.* **1981**, *103*, 36. (y) Franke, W.; Frenking, G.; Schwarz, H.; Wolfschütz, R. *Chem. Ber.* **1981**, *114*, 3878.

(8) For pertinent literature concerning the MIKES technique (mass analyzed ion kinetic energy spectroscopy) see: (a) Beynon, J. H.; Cooks, R. G.; Amy, J. W.; Baitinger, W. E.; Ridley, T. Y. *Anal. Chem.* **1973**, *45*, 1023A. (b) Schlunegger, U. P. *Angew. Chem., Int. Ed. Engl.* **1975**, *14*, 679. (c) Beynon, J. H.; Cooks, R. G. In "Mass Spectrometry, International Review of Science"; Maccoll, A., Ed.; Butterworths: London, 1975. (d) Cooks, R. G.; Beynon, J. H.; Caprioli, R. M.; Lester, G. R. "Metastable Ions"; Elsevier; Amsterdam, 1973.

Table III. Collisional Activation Mass Spectra of $C_2H_4Cl_2^{+\cdot}$ (m/z 98, $^{35}Cl_2$) and $C_2H_4Br_2^{+\cdot}$ (m/z 188, $^{81}Br^{79}Br$) Formed from Several Precursors[a,b]

fragment ions, m/z	$CH_3CHCl_2^{+\cdot}$ (10)	$CHCl_2CO_2CH_3^{+\cdot} \xrightarrow{-CO_2}$ 5 $C_2H_4Cl_2^{+\cdot}$	fragment ions, m/z	$CH_3CHBr_2^{+\cdot}$ (11)	$CHBr_2CO_2CH_3^{+\cdot} \xrightarrow{-CO_2}$ 6 $C_2H_4Br_2^{+\cdot}$
83	36	87	173[c]	33	707
63[c]	1881	92	160	23	0.7
61[c]	26	1.9	109[c]	1131	57
48	8.4	6.1	107[c]	1127	57
47	7.3	5.3	93	24	49
36	2.3		91	21	44
35	10		81	12	2.3
27	36	1.8	79	11	2.2
			27	9.7	1.3

[a] The spectra were recorded by using the MIKES method[8]. [b] See footnote *a* of Table I. [c] See footnote *b* of Table I.

On the other hand, the CA spectra of the $C_2H_4X_2^{+\cdot}$ ions, generated from **5** and **6**, are dominated by $CH_3\cdot$ loss, and we suggest that the $[M - CO_2]^{+\cdot}$ fragment ions are best represented by structures **12** and **13**. The two sets of isomeric $C_2H_4X_2^{+\cdot}$ structures do not interconvert on the time scale of the mass spectrometer.

To the best of our knowledge it seems that *8*, *9*, *12*, and *13* are the first cases of haloalkane cation radicals containing a *divalent* halogen atom X (X = Cl, Br) bonded to two carbons.[9,10] The unusual constitution of these ions prompted us to investigate their geometries, energies, and mechanism of formation by means of molecular orbital calculations.

Molecular Orbital Calculations. Quantum mechanical calculations can provide insight into the experimental results. As these calculations usually describe the isolated molecules, they are ideally suited for comparisons with gas-phase experiments. Indeed, numerous examples are now available that demonstrate the advantages of combined experimental/theoretical investigation for gas ion studies.[11] We use here both the semiempirical MNDO method[12a] and standard ab initio methods[12b] with various basis sets.[13a-d] MNDO uses the restricted Hartree–Fock approximation (RHF) while with the ab initio calculations we have used the unrestricted Hartree–Fock procedures (UHF).[13e] The effect of correlation energy was evaluated by using the second-order Møller–Plesset perturbation theory (UMP2).[13f,g] The transition states were rigorously defined (one and only one negative eigenvalue of the force-constant matrix) and located according to the procedures described in the literature.[14] Combination of MNDO and the ab initio methods provides an effective procedure for searching potential-energy surfaces. MNDO is a fast and reliable

Table IV. Calculated Heats of Formation (MNDO, kcal mol^{-1}), Total Energies (hartrees), and Relative Energies (kcal mol^{-1}) of the Isomeric $C_2H_5Cl^{+\cdot}$ Ions 6 and 8

computational method[a]	$CH_3CH_2Cl^{+\cdot}$ (6)	$CH_3ClCH_2^{+\cdot}$ (8)
MNDO		
ΔH_f°	245.2	235.1
rel energy	0	−10.1
4-31G/MNDO		
total energy	−537.128 99	−537.131 17
rel energy	0	−1.4
STO-3G/STO-3G		
total energy	−531.980 99	−531.953 28
rel energy	0	17.4
4-31G/STO-3G		
total energy	−537.168 67	−537.131 68
rel energy	0	23.2
6-31G*/STO-3G		
total energy	−537.764 42	−537.745 86
rel energy	0	11.6
6-31G*/6-31G*[b]		
total energy	−537.763 94	−537.749 43
rel energy	0	9.1
UMP2/6-31G*//STO-3G		
total energy	−538.141 53	−538.131 38
rel energy	0	6.4

[a] The designation 4-31G/MNDO denotes the calculated energy at 4-31G with the MNDO optimized geometry. Similarly, 6-31G*/STO-3G gives the 6-31G* energy at the STO-3G geometry, etc. [b] With the optimized STO-3G geometries except that the C–Cl bond length, the CCCl bond angle in 6, and the CClC bond angle in 8 were reoptimized at 6-31G* (see Chart I).

(9) Preliminary communications on $CH_3XH^{+\cdot}$ and its isomeric form $CH_2XH_2^{+\cdot}$ (X = O, S, NH, F, Cl, Br) were reported recently: (a) Bouma, W. J.; Nobes, R. H.; Radom, L. *J. Am. Chem. Soc.* **1982**, *104*, 2929. (b) Bouma, W. J.; MacLeod, J. K.; Radom, L. *Ibid.* **1982**, 104, 2930. (c) Holmes, J. L.; Lossing, F. P.; Terlouw, J. K.; Burgers, P. C. *Ibid.* **1982**, 104, 2931. (d) Halim, H.; Ciommer, B.; Schwarz, H. *Angew. Chem., Int. Ed. Engl.* **1982**, *21*, 528. (e) Bouma, W. J.; Yates, B. F.; Radom, L. *Chem. Phys. Lett.*, in press. (f) Bouma, W. J.; Dawes, J. M.; Radom, L. *Org. Mass Spectrom.*, in press.

(10) For divalent closed-shell halonium ions see: (a) Olah, G. A.; Mo, Y. K. In "Carbonium Ions"; Olah, G. A., Schleyer, P. v. R., Eds.; Wiley-Interscience: New York, 1976; Vol V, 2135. (b) Radom, L.; Poppinger, D.; Haddon, R. C. *Ibid.* 2303.

(11) See (a) ref 7d,f,s,t,y. (b) Apeloig, Y.; Collins, J. B.; Cremer, D.; Bally, T.; Haselbach, E.; Pople, J. A.; Chandrasekhar, J.; Schleyer, P. v. R. *J. Org. Chem.* **1980**, *45*, 3496. (c) Bouchoux, G.; Hoppiliard, Y. *Org. Mass Spectrom.* **1981**, *16*, 459. (d) Dewar, M. J. S.; Rzepa, H. S. *J. Am. Chem. Soc.* **1977**, *99*, 7432. (e) Krause, D. A.; Day, R. J.; Jorgensen, W. L.; Cooks, R. G. *Int. J. Mass Spectrom. Ion Phys.* **1978**, *27*, 227. (f) Day, R. J.; Krause, D. A.; Jorgensen, W. L.; Cooks, R. G. *Ibid.* **1979**, *30*, 83. (g) Frenking, G.; Schmidt, J.; Schwarz, H. *Z. Naturforsch. B, Anorg. Chem., Org. Chem., Biochem., Biol.* **1980**, *35B*, 1031. (h) Dill, J. D.; McLafferty, F. W. *J. Am. Chem. Soc.* **1979**, *101*, 6526. (i) Sannen, C.; Raseev, G.; Galloy, C.; Fauville, G.; Lorquet, J. C. *J. Chem. Phys.* **1981**, *74*, 2402. (j) Ciommer, B.; Frenking, G.; Schwarz, H. *Chem. Ber.* **1981**, *114*, 1503. (k) Bouma, W. J.; MacLeod, J. K.; Radom, L. *J. Am. Chem. Soc.* **1980**, *102*, 2246. (l) Baumann, B. C.; MacLeod, J. K.; Radom, L. *Ibid.* **1980**, *102*, 7927. (m) Day, R. J.; Cooks, R. G. *Int. J. Mass Spectrom. Ion Phys.* **1980**, *35*, 293. (n) Franke, W; Schwarz, H.; Thies, H.; Chandrasekhar, J.; Schleyer, P. v. R.; Hehre, W. J.; Saunders, M.; Walker, G. *Chem. Ber.* **1981**, *114*, 2808. (o) Tasaka, R.; Ogata, M.; Ichikawa, H. *J. Am. Chem. Soc.* **1981**, *103*, 1885. (p) Houriet, R.; Schwarz, H.; Zummack, W.; Andrade, J.; Schleyer, P. v. R. *Nouv. J. Chim.* **1981**, *5*, 505. (q) Frenking, G.; Schwarz, H. *Comput. Chem.* **1982**, *3*, 251. (r) Frenking, G.; Schmidt, J.; Schwarz, H. *Z. Naturforsch. B, Anorg. Chem., Org. Chem., Biochem., Biol.* **1982**, *37B*, 355. (s) Wolfschütz, R.; Halim, H.; Schwarz, H. *Ibid.* **1982**, *37B*, 724. (t) Heinrich, N.; Wolfschütz, R.; Frenking, R.; Schwarz, H. *Int. J. Mass Spectrom. Ion Phys.* **1982**, *44*, 81. (u) Thies, H.; Wolfschütz, R.; Frenking, G.; Schmidt, J.; Schwarz, H. *Tetrahedron* **1982**, *38*, 1647. (v) Würthwein, E. U.; Halim, H.; Schwarz, H.; Nibbering, N. M. M. *Chem. Ber.* **1982**, *115*, 2626. (w) Bentley, T. W.; Wellington, C. A. *Org. Mass Spectrom.* **1981**, *12*, 523. (x) Hoppiliard, Y.; Bouchoux, C., Jaudon, P. *Nouv. J. Chim.* **1982**, *6*, 43. (y) Holzmann, G.; Frenking, G.; Steiner, B. *Org. Mass Spectrom.* **1982**, *17*, 455. (z) Bouma, W. J.; Nobes, R. H.; Radom, L. *Ibid.* **1982**, *17*, 315.

(12) (a) Dewar, M. J. S.; Thiel, W. *J. Am. Chem. Soc.* **1977**, *99*, 4889, 4907; Program No. 353, Quantum Chemistry Program Exchange (QCPE), Indiana University, Bloomington, IN. (b) For the ab initio calculations the GAUSSIAN-76 and the GAUSSIAN-80 series of programs were used. Programs 368 and 406, respecively, QCPE.

(13) STO-3G: (a) Hehre, W. J.; Stewart, R. F.; Pople, J. A. *J. Chem. Phys.* **1969**, *51*, 2657. (b) Hehre, W. J.; Ditchfield, R.; Stewart, R. F.; Pople, J. A. *Ibid.* **1970**, *52*, 2679. 4-31G: (c) Ditchfield, R.; Hehre, W. J.; Pople, J. A., *Ibid.* **1971**, *54*, 724. 6-31G*: (d) Francl, M. M.; Pietro, W. J.; Hehre, W. J.; Binkely, J. S.; Gordon, M. S.; De Frees, D. J.; Pople, J. A. *J. Chem. Phys.* **1982**, *77*, 3654. (e) Pople, J. A.; Nesbet, R. K. *Ibid.* **1954**, *27*, 571. (f) Møller, C.; Plesset, M. S. *Phys. Rev.* **1974**, *46*, 1423. (g) Binkley, J. S.; Pople, J. A. *Int. J. Quantum Chem.* **1975**, *9*, 229. (h) Davidson, W. C. *Comput. J.* **1968**, *10*, 406. (i) Fletcher, R.; Powell, M. J. D. *Ibid.* **1963**, *6*, 163. (j) Poppinger, D. *Chem. Phys. Lett.* **1975**, *34*, 332.

(14) (a) Powell, M. J. D. *Comput. J.* **1965**, *7*, 303. (b) Murrell, J. N.; Laidler, K. J. *Trans. Faraday Soc.* **1968**, *64*, 371. (c) McIver, J. W., Jr. *Acc. Chem. Res.* **1974**, *7*, 71. (d) Poppinger, D. *Chem. Phys. Lett.* **1975**, *35*, 550.

Chart I

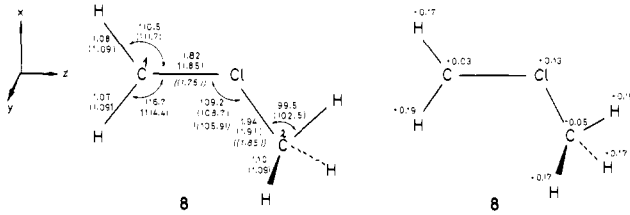

Bond lengths in Å and angles in °, MNDO (STO-3G) ((6-31G*)) Total charges (STO-3G)

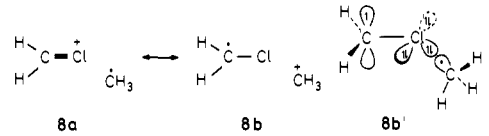

8a 8b 8b'

Chart II

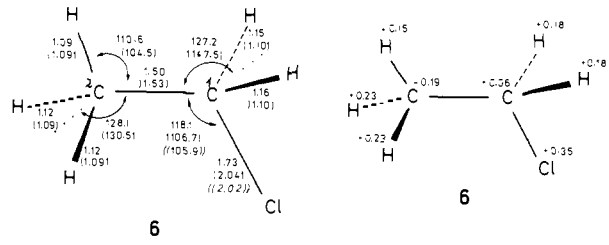

Bond lengths in Å and angles in °, MNDO (STO-3G) ((6-31G*)) Total charges (STD-3G)

method for geometry optimizations. These optimized geometries are then used in single-point ab initio calculations for obtaining more accurate relative energies. Recent studies[15a] suggest that this strategy is useful for calculating properties of ionic species. Although the computational experience with hypervalent open-shell ions such as **8** is limited, we believe that the results of our calculations are significant (see also below). Recent studies have shown that both MINDO/3[16a] and ab initio calculations at the STO-3G and the 4-31G levels[16b-d] of ions of the general type RXR'^{+} (X = F, Cl; R or R' = H, alkyl) are generally in good agreement with experiment. It is also encouraging that the calculated ionization potentials of alkyl chlorides correlate reasonably well with the experimental values.[16e,f]

We have confined the calculations to the $C_2H_5Cl^{+}\cdot$ system, as no parameters are available for bromine. Economical constraints exclude a theoretical study of the $C_2H_4Cl_2^{+}\cdot$ cations. However, we believe that the important structural features of these novel halonium ions and their mode of formation can be revealed by analysis of the parent $C_2H_5Cl^{+}\cdot$ system.

The geometries of ions **6** and **8** were optimized with MNDO[12] and with the minimal STO-3G basis set[13a] using analytically evaluated atomic forces.[13h-j,14d] Partial geometry optimizations were also carried out at 6-31G*.[13d] Both species were found to exist in minima on the potential-energy surface. MNDO favors the halonium ion **8** over the ionized chloroethane **6** by 10 kcal mol^{-1}, whereas **6** is substantially more stable than **8** according to the STO-3G, 4-31G, 6-31G*, and the UMP2/6-31G* calculations (Table IV).[16e,f]

Both the STO-3G and the 4-31G basis sets underestimate the stability of the nonclassical chloronium cations radical **8**. The addition of a set of d functions lowers substantially the energy of **8** relative to **6**. This is expected because **8** is an hypervalent molecule where the flexibility of the basis set and in particular d functions are more important than for the classical structure of ion **6**.[13d,15b] At 6-31G*/STO-3G (i.e., a single-point 6-31G* calculation at the optimized STO-3G geometry) **8** is less stable than **6** by 11.4 kcal mol^{-1}. Partial geometry optimization (i.e., of the C–Cl bond lengths, the CCCl bond angle in **6**, and the CClC bond angle in **8**) lowers the energy of **8** relative to **6** by only 2.3 kcal mol^{-1} (Table IV). Inclusion of correlation energy has a relatively little effect on the energy difference between **6** and **8**. At UMP2/6-31G*, the highest theoretical level that we have used, **6** is more stable than **8** by ca. 6.4 kcal mol^{-1}. We believe[16a-d] that **6** will remain more stable than **8** also at higher levels of theory.

The structure of the chloronium radical ion **8** deserves attention since it accounts for some of the experimental observations. First, we note that the MNDO and the STO-3G optimized structures of **8** are very similar (Chart I). Both methods predict that **8** is a bent cation radical ($\angle C^1ClC^2 = 106°$) with unequal C–Cl bond lengths. **8** can be described as the product of hydrogen abstraction from the dimethylchloronium cation, $(CH_3)_2Cl^{+}$, where the two C–Cl bond lengths are equal. Qualitatively, **8** can be described as a resonance hybrid of structures **8a** and **8b**. The calculations suggest that hybrid **8b**, which describes a complex between the chloromethyl radical ($CH_2Cl\cdot$) and the methyl cation (CH_3^{+}), is the major contributing structure. For example, the geometry of **8** resembles closely the structure that is expected for **8b**. The C^1–Cl bond is significantly shorter than the C^2–Cl bond at all theoretical levels, i.e., 1.82 vs. 1.94 Å at MNDO, 1.85 vs. 1.90 Å at STO-3G, and 1.76 vs. 1.85 Å at 6-31G* (Chart I and Table IV). For comparison the C–Cl bond lengths in CH_2Cl^{+}, $CH_2Cl\cdot$, and $CH_2ClH^{+}\cdot$ are 1.68, 1.77, and 1.88 Å (STO-3G). If structure **8a** contributes significantly, then **8** would have a much shorter C^1–Cl bond length than is actually observed. The C^1–Cl bond in **8** lengthens by 0.07 Å (compared to $CH_2Cl\cdot$) as a result of the complexation with the methyl cation. A similar C–Cl bond lengthening is obseved upon protonation of $CH_2Cl\cdot$. The bond angles around C^1 in **8** and in $CH_2Cl\cdot$ are almost identical. The charge and spin distribution also point to the major role of structure **8b**.[17a] The charge at chlorine in **8** (+0.13) is much smaller than in CH_2Cl^{+} (+0.28) but similar to that in CH_3ClH^{+} (+0.15)[16d] and in $CH_2ClH^{+}\cdot$ (+0.18). The somewhat smaller charge on Cl in **8** relative to CH_3ClH^{+} and $CH_2ClH^{+}\cdot$ results mainly from the larger number of hydrogens in **8**, which allow a more effective dispersal of the charge. In fact, the positive charge in **8** is located mainly at the hydrogens, approximately +0.17 at each hydrogen (Chart I[17a]). The spin density in **8** is located primarily at the $2p_y$ orbital of C^1 (i.e., 0.98 electrons), also supporting the analogy with $CH_2Cl\cdot$ and $CH_2ClH^{+}\cdot$, which behave similarly. MNDO bond indices[17b] and STO-3G overlap populations also indicate that the C^1–Cl bond is essentially a regular C–Cl single bond, as implied by structure **8b**, while the C^2–Cl bond is much weaker (MNDO bond indices: 0.90 vs. 0.64). The weak C^2–Cl bond in **8** and the fact that the radical center is located at C^1, i.e., α to the C^2–Cl bond, are both consistent with the observed facile loss of $CH_3\cdot$. Expulsion of a methyl radical from **8** is also favored thermochemically over that of CH_3^{+}, as the experimentally derived heats of formation for the pair ($CH_3\cdot$ + CH_2Cl^{+}) is lower by 12 kcal mol^{-1} than that of ($CH_2Cl\cdot$ + CH_3^{+}).[18a] In conclusion, in terms of simple molecular orbital theory **8** is best described as a complex (i.e., **8b**) between $CH_2Cl\cdot$ and CH_3^{+}, where the electrophile is bonded by the chlorine's lone pairs (**8b'**).

(15) (a) Köhler, H. J.; Lischka, H. *J. Am. Chem. Soc.* **1978**, *100*, 5279; **1979**, *101*, 3479 and references therein. (b) Similarly, it is well-known that nonclassical structures (e.g., bridged ions) are stabilized relative to the isomeric classical structures by the addition of d functions. See, for example, ref 11d and references therein, and also: Pople, J. A. *Int. J. Mass Spectrom. Ion Phys.* **1975**, *19*, 89. Radom, L.; Hariharan, P. C.; Pople, J. A.; Schleyer, P. v. R. *J. Am. Chem. Soc.* **1973**, *95*, 6531.

(16) (a) McManus, S. P. *J. Org. Chem.* **1982**, *47*, 3070. (b) Jorgensen, W. L. *J. Am. Chem. Soc.* **1977**, *99*, 280, 4272; **1978**, *100*, 1049. (c) Jorgensen, W. L.; Munroe, J. E. *Tetrahedron Lett.* **1977**, 581. (d) Jorgensen, W. L., *J. Am. Chem. Soc.* **1978**, *100*, 1057. (e) For example, the calculated ionization potential (IP, in eV) of CH_3Cl is 12.25 (MNDO), 10.36 (STO-3G),[16d] 11.70 (4-31G),[16d] and 11.83 (6-31G*), compared to the experimental value of 11.27 eV. Other alkyl chlorides behave similarly.[16a-d] Note that the MNDO-calculated IP is substantially too high. (f) The failure of MNDO may be due to a poor description of $CH_3CH_2Cl^{+}\cdot$ that results in the underestimation of its stability. The deficiency is exemplified by the high calculated IP of $CH_3CH_2Cl^{+}\cdot$ (12.11 eV compared to the experimental value of 10.97 eV).

(17) (a) The analysis is based on the STO-3G calculations. The 6-31G* calculations lead to the same conclusions. (b) Bond indices were calculated according to Armstrong et al.: Armstrong, D. R.; Perkins, P. G.; Steward, J. J. P. *J. Chem. Soc., Dalton Trans.* **1973**, 838.

Scheme I

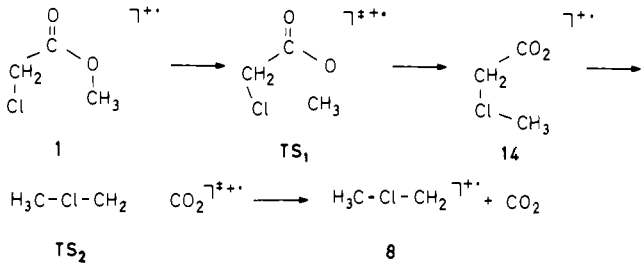

Scheme II

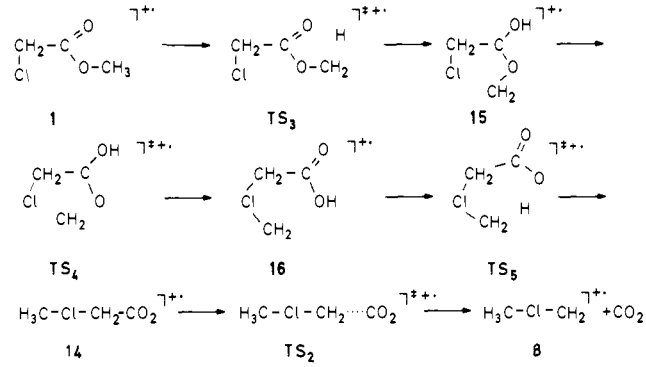

Scheme III

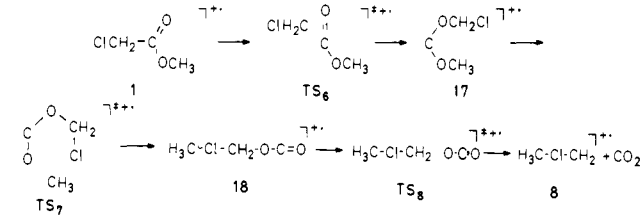

6 is best described as being obtained by the removal of one electron out of the chlorine's lone pair electrons. Indeed the spin density is located entirely on chlorine. The positive charge is dispersed over the entire molecule but one third of the positive charge is still located at chlorine (Chart II). We believe that the ionization of CH_3CH_2Cl results in a significant elongation of the C–Cl bond as the STO-3G (1.81 → 2.04 Å) and the 6-31G* (2.02 Å in **6**) calculations predict. According to MNDO the C–Cl bond in $CH_3CH_2Cl^{+\cdot}$ is shorter by 0.07 Å than in CH_3CH_2Cl,[18b] but such strengthening of the C–Cl bond upon ionization is not consistent with the experimentally observed facile dissociation of $CH_3CH_2Cl^{+\cdot}$ to $CH_3CH_2^+$ and Cl·. In addition, C^1 approaches planarity upon ionization as expected for a longer partially ionized C–Cl bond. The C^2C^1X angle (X is a point along the bisector of the HC^1H angle) in **6** is 147.5°, much larger than around a perfect tetrahedral center (125.3°).

To determine the energetically most feasible pathway for the generation of $CH_3ClCH_2^{+\cdot}$ and CO_2 from ionized methyl chloroacetate, we considered three possible mechanisms for the unimolecular CO_2 loss from $\mathbf{1}^{+\cdot}$ (Schemes I–III). In the reaction path given in Scheme I the methyl group is transferred as one intact unit via transition state TS_1 to the chlorine; the resulting intermediate **14** dissociates to **8** and CO_2 by C–C bond fission via TS_2. The second reaction path (Scheme II) commences with a hydrogen transfer[19] from the methyl group to the carbonyl oxygen atom (**1** → TS_3 → **15**). The resulting intermediate **15** rearranges further by a methylene transfer to chlorine (**15** → TS_4 → **16**). This step is followed by a back-transfer of the hydroxylic hydrogen to the terminal CH_2 group via TS_5, generating **14**, which dissociates to **8** and CO_2. The third reaction path (Scheme III) requires the transfer of the intact CH_2Cl group to the ionized carbonyl function (**1** → TS_6 → **17**), followed by a CH_3 migration (**17** → TS_7 → **18**) and fission of the C–O bond (**18** → TS_8 → **8** + CO_2). The geometries and the energies of the various transition states and intermediates that are involved in these three reaciton paths were obtained by complete geometry optimization[20] using the MNDO method. The relevant data are given in Table V.

Scheme IV. Part of the Potential-Energy Surface for the Decomposition of $ClCH_2CO_2CH_3^{+\cdot}$ to CO_2 + $CH_3ClCH_2^{+\cdot}$.[a]

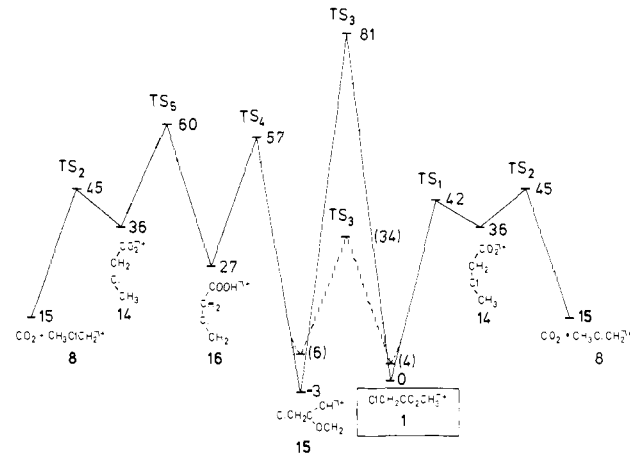

[a] The indicated energies (kcal mol^{-1}) are relative to $ClCH_2CO_2$-$CH_3^{+\cdot}$. Values are according to the 4-31G/MNDO calculations (corrected 4-31G/MNDO values are given in parentheses). The solid and the dotted lines refer to the 4-31G/MNDO and the corrected 4-31G/MNDO calculations, respectively.

The calculated heats of formation (MNDO) of the various transition states (Table V) suggest that the three pathways contribute to the formation of $CH_3ClCH_2^{+\cdot}$ and CO_2 to a similar extent. Thus, the highest transition states along the pathways of Schemes I–III are all comparable in energy, i.e., TS_2 = 220 kcal mol^{-1} for pathway I, TS_5 = 222 kcal mol^{-1} for pathway II, and $TS_7 \simeq$ 210 kcal mol^{-1} for pathway III. However, a closer inspection of the reaction intermediates indicates that only pathway I contributes to the generation of $CH_3ClCH_2^{+\cdot}$; pathways II and III can be excluded. Consider first pathway II (Scheme II). Even if **16** is formed, it is unlikely to rearrange via TS_5 to **14**. **16** is more likely to dissociate by cleavage of the weak C^2–Cl bond via TS_{11}, which is substantially lower in energy (ΔH_f° = 172 kcal mol^{-1}) then TS_5 (ΔH_f° = 222 kcal mol^{-1}). Similar considerations exclude also pathway III (Scheme III) as an important route for the generation of **8**. Thus, elimination from **17** of either CH_3· via TS_9 or CH_2Cl· via TS_{10} requires much less energy than the rearrangement of **17** via TS_7 to **18** (i.e., by 20 and 36 kcal mol^{-1}, respectively). Furthermore, even if **18** is formed, it is expected, as a result of the very weak CH_2–$ClCH_3$ bond (2.11 Å, Table V), to eliminate CH_3Cl. There is no experimental evidence, however, for the elimination of CH_3Cl from $\mathbf{1}^{+\cdot}$. Thus, although **18** is a stable species, it is probably not formed during the elimination of CO_2 from $\mathbf{1}^{+\cdot}$. We have also studied several other possibilities for CO_2 loss from $\mathbf{1}^{+\cdot}$, but these reaction paths were all higher in energy than path I.

The entire evidence of the MNDO results suggests that the unimolecular loss of CO_2 from $\mathbf{1}^{+\cdot}$ proceeds via pathway I (Scheme I), although TS_2, TS_5, and TS_7 are close in energy. Since MNDO is not parameterized for open-shell ions and as it represents a

(18) (a) Rosenstock, H. M.; Draxl, K.; Steiner, B. W.; Herron, J. T. *J. Phys. Chem. Ref. Data* **1977**, Vol. 6. (b) For comparison note that the C–Cl bond length in CH_3CH_2Cl is the same (1.81 Å) at STO-3G[16] and at MNDO.

(19) Convincing evidence has been presented in recent review articles for the operation of similar kinds of "hidden" hydrogen rearrangements; see: (a) Schwarz, H. *Nachr. Chem. Techn. Lab.* **1980**, *28*, 158. (b) Bar-Shai, R.; Bortinger, A.; Sharvit, J.; Mandelbaum, A. *Isr. J. Chem.* **1980**, *20*, 137. (c) Schwarz, H. *Org. Mass Spectrom.* **1980**, *15*, 491. (d) Schwarz, H. *Top. Curr. Chem.* **1981**, *97*, 1.

(20) This does not hold for TS_7, which we were unable to define rigorously as a transition state. The heat of formation of TS_7 is estimated to be ca. 210 kcal mol^{-1} (MNDO).

Table V. Calculated (MNDO) Heats of Formation (kcal mol^{-1}), Geometries (Bond Lengths in Å, Angles in deg), and Charge Distributions for Some Ionic Intermediates and Transition States[a]

structure	ΔH_f°, kcal mol^{-1}	selected geometry data		charge distribution	
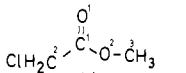 **1**$^{1+\cdot}$	158	C^1O^1	1.31	O^1	0.03
		C^1O^2	1.29	O^2	−0.17
		C^1C^2	1.54	C^1	0.38
		O^2C^3	1.45	C^2	0.07
		C^2Cl	1.77	C^3	0.20
		$O^1C^1O^2$	112	Cl	0.02
		$C^2C^1O^1O^2$	180		
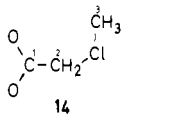 **14**	189	C^1O	1.27	O	−0.08
		C^1C^2	1.54	C^1	0.22
		C^2Cl	1.91	C^2	0.17
		C^3Cl	1.94	C^3	0.27
		OC^1O	120	Cl	0.03
		C^2ClC^3	113		
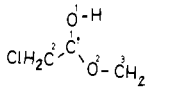 **15**	112	C^1O^1	1.32	O^1	−0.13
		C^1O^2	1.34	O^2	−0.08
		C^1C^2	1.52	C^1	0.24
		C^2Cl	1.78	C^2	0.07
		$O^1C^1O^2$	107	C^3	0.22
		$O^1C^1O^2C^3$	180	Cl	−0.06
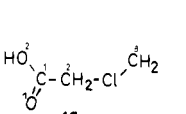 **16**	158	C^1O^1	1.22	O^1	−0.24
		C^1O^2	1.35	O^2	−0.30
		C^1C^2	1.53	C^1	0.30
		C^2Cl	1.94	C^2	0.22
		C^3Cl	1.82	C^3	0.07
		$O^1C^1O^2$	123	Cl	0.16
		$O^1C^1O^2C^2$	180		
		C^2ClC^3	111		
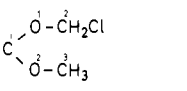 **17**	145	C^1O^1	1.25	O^1	−0.16
		C^1O^2	1.27	O^2	−0.16
		C^2O^1	1.45	C^1	0.49
		C^3O^2	1.45	C^2	0.25
		C^2Cl	1.78	C^3	0.23
		$O^1C^1O^2$	138	Cl	−0.09
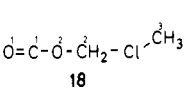 **18**	168	C^1O^1	1.16	O^1	0.07
		C^1O^2	1.25	O^2	−0.12
		C^2O^2	1.42	C^1	0.58
		C^2Cl	2.11	C^2	0.15
		C^3Cl	1.90	C^3	0.20
		$O^1C^1O^2$	180	Cl	−0.29
		C^2ClC^3	174		
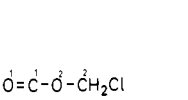 **19**	140	C^1O^1	1.15	O^1	0.11
		C^1O^2	1.26	O^2	−0.16
		C^2O^2	1.46	C^1	0.59
		C^2Cl	1.77	C^2	0.28
		$O^1C^1O^2$	180	Cl	−0.06
		$C^1O^2C^2$	129		
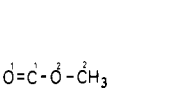 **20**	142	C^1O^1	1.16	O^1	0.09
		C^1O^2	1.25	O^2	−0.15
		C^2O^2	1.47	C^1	0.58
		$O^1C^1O^2$	180	C^2	0.25
		$C^1O^2C^2$	129		
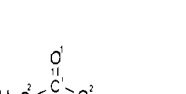 **TS$_1$**	220	C^1O^1	1.26	O^1	−0.02
		C^1O^2	1.26	O^2	−0.38
		C^1C^2	1.59	C^1	0.32
		C^2Cl	1.80	C^2	0.15
		C^3O^2	2.05	C^3	0.53
		C^3Cl	2.40	Cl	−0.09
		O^2C^3Cl	77		
		RC: C^3–O^2			
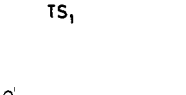 **TS$_2$**	205	OC^1	1.22	O^1	−0.10
		C^1C^2	1.79	O^2	−0.22
		C^2Cl	1.86	C^1	0.28
		C^3Cl	1.97	C^2	0.20
		$O^1C^1O^2$	144	C^3	0.29
		C^2ClC^2	114	Cl	0.04
		RC: C^1–C^2			
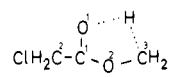 **TS$_3$**	180	C^1O^1	1.29	O^1	−0.13
		C^1O^2	1.33	O^2	−0.21
		C^1C^2	1.53	C^1	0.39
		C^2Cl	1.78	C^2	0.11
		C^3O^2	1.43	C^3	0.24
		C^3H	1.25	Cl	−0.03
		O^1H	1.55		
		O^1HC^3	154		
		$O^1C^1C^2$	112		
		RC: H–C^3			
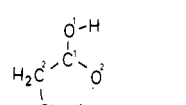 **TS$_4$**	181	C^1O^1	1.34	O^1	−0.20
		C^1O^2	1.24	O^2	−0.23
		C^1C^2	1.53	C^1	0.35
		C^2Cl	1.77	C^2	0.16
		C^3O^2	2.00	C^3	0.07
		C^3Cl	1.94	Cl	0.13
		O^2C^3Cl	100		
		RC: C^3–O^2			
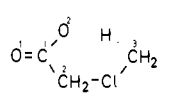 **TS$_5$**	222	C^1O^1	1.22	O^1	−0.18
		C^1O^2	1.35	O^2	−0.18
		C^1C^2	1.53	C^1	0.26
		C^2Cl	1.91	C^2	0.17
		C^3Cl	1.89	C^3	0.19
		C^3H	1.24	Cl	0.08
		O^2H	1.30		
		O^2HC^3	159		
		RC. H–C^3			
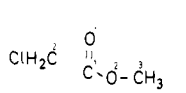 **TS$_6$**	203	C^1O^1	1.24	O^1	−0.16
		C^1O^2	1.28	O^2	−0.15
		C^3O^2	1.44	C^1	0.31
		C^1C^2	1.95	C^2	0.38
		C^2O^1	1.86	C^3	0.22
		C^2Cl	1.77	Cl	−0.05
		$O^1C^1C^2$	38		
		$O^1C^1O^2$	132		
		RC: C^2–O^1			
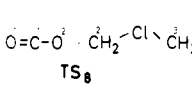 **TS$_8$**	180	C^1O^1	1.17	O^1	−0.10
		C^1O^2	1.20	O^2	−0.32
		C^2O^2	1.91	C^1	0.51
		C^2Cl	1.92	C^2	0.28
		C^3Cl	1.89	C^3	0.23
		$O^1C^1O^2$	180	Cl	−0.02
		C^2ClC^3	115		
		RC: C^2–O^2			
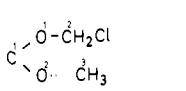 **TS$_9$**	190	C^1O^1	1.27	O^1	−0.18
		C^1O^2	1.19	O^2	−0.18
		C^2O^1	1.45	C^1	0.39
		C^2Cl	1.79	C^2	0.26
		C^3O^2	2.41	C^3	0.40
		$O^1C^1O^2$	152	Cl	−0.13
		RC: C^3–O^2			
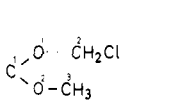 **TS$_{10}$**	174	C^1O^1	1.19	O^1	−0.11
		C^1O^2	1.28	O^2	−0.16
		C^2O^1	2.20	C^1	0.41
		C^2Cl	1.71	C^2	0.21
		C^3O^2	1.45	C^3	0.22
		$O^1C^1O^2$	148	Cl	0.02
		RC: C^2–O^1			
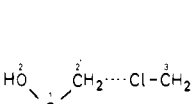 **TS$_{11}$**	172	C^1O^1	1.22	O^1	−0.24
		C^1O^2	1.35	O^2	−0.32
		C^1C^2	1.51	C^1	0.31
		C^2Cl	2.34	C^2	0.21
		C^3Cl	1.72	C^3	0.23
		RC: C^2–Cl		Cl	0.08

[a] RC in the transition-state geometries defines the reaction coordinate chosen in the calculations.

Table VI. Calculated Total Energies (4-31G/MNDO, hartrees) and Relative Energies (kcal mol^{-1}, referred to 1$^+$) of Selected Intermediates and Transition States for CO_2 Loss from 1$^{+\cdot}$[a]

species	4-31G (total)	4-31G (rel)	MNDO (rel)
1$^{+\cdot}$	−724.480 52 (−724.473 57)	0 (4)	0
14	−724.423 26	36	31
15	−724.484 53 (−724.471 58)	−3 (6)	−46
16	−724.438 27	27	0
17	−724.456 49 (−724.444 39)	15 (23)	−13
CO_2	−187.324 71	15	2
8	−537.131 17	15	2
TS_1	−724.413 53	42	62
TS_2	−724.409 50	45	47
TS_3	−724.351 58 (−724.425 85)	81 (34)	22
TS_4	−724.389 85	57	23
TS_5	−724.384 80	60	64
TS_6	−724.370 32 (−724.368 39)	69 (70)	45

[a] Values in parentheses refer to the corrected 4-31G/MNDO calculations.

relatively simple level of theory, we have calculated the most relevant parts of the potential energy surface by ab initio methods. Single-point calculations with the 4-31G basis set at the MNDO-optimized geometries (i.e., 4-31G/MNDO) were performed. Experience shows that the split-valence 4-31G basis set is usually reliable for predicting the relative energies of isomers.[21] The close similarity in the MNDO and the STO-3G structures of **8** supports the use of the MNDO geometries for the ab initio calculations. This is not the case, however, for $CH_3CH_2Cl^{+\cdot}$, where we find a very large difference between the MNDO and STO-3G calculated C–Cl bond lengths (1.734 and 2.04 Å). Such a large difference in geometry might result in a significant change in energy. For the species that contain the $CH_2Cl^{+\cdot}$ unit (e.g., **1**$^{+\cdot}$, **15**, **17**, TS_3, and TS_6) we have therefore performed also single-point 4-31G calculations at the MNDO-optimized geometries, but with C–Cl bond lengths of 2.04 Å (these energies are denoted as "corrected" 4-31G/MNDO values). The corrected 4-31G/MNDO calculations show (Table VI, values in parentheses) that while the energies of **1**$^{+\cdot}$, **15**, **17**, and TS_6 are relatively insensitive to changes in the C–Cl bond length, the energy of TS_3 is lowered dramatically by the elongation of the C–Cl bond to 2.04 Å. Thus, at the corrected 4-31G/MNDO level, TS_3 is 30 kcal mol^{-1} higher in energy than **1**$^{+\cdot}$, and 12 and 15 kcal mol^{-1} lower in energy than TS_1 and TS_2, respectively (Table VI and Scheme IV). Note, however, that the energies of TS_4 and TS_5, which are of the bridged chloronium type (as are TS_1 and TS_2), should not be affected by this correction procedure. Thus, according to the corrected 4-31G/MNDO values the rate-determining transition state along reaction path II is either TS_4 or TS_5 and *not* the initial hydrogen-transfer step (i.e., TS_3) as suggested by the 4-31G/MNDO calculations. It is obvious from this dependency of the results on the computational method that at the present level of theory the energy diagram (Scheme IV) must be regarded only as a semiquantitative guide. More elaborate calculations, which are beyond our present resources, must be carried out for obtaining more reliable quantitative results. We believe strongly, however, that the central conclusion of both the 4-31G and the MNDO calculations,[22] namely, that the favored mechanism for the formation of $CH_3ClCH_2^{+\cdot}$ from **1**$^{+\cdot}$, is best represented by path I (Scheme I), will hold at higher levels of theory. Thus the highest point on the potential-energy surface along path I (TS_2) is lower in energy than the highest points along path II (i.e., TS_5) and path III (i.e., TS_6) by 15 and 24 kcal mol^{-1}, respectively (corrected 4-31G/MNDO values, Table VI). Selected parts of the potential-energy surface along pathes I and II, according to the 4-31G/MNDO and the corrected 4-31G/MNDO calculations, are presented in Scheme IV. We estimate that the activation energy for the dissociative rearrangement of **1**$^{+\cdot}$ to **8** via path I is lower than the 4-31G/MNDO estimate of 40–45 kcal mol^{-1} (Scheme IV). Our experience with **6** and **8** (see above) suggests that the 4-31G basis set underestimates the stabilities of TS_1 and TS_2, which contain a bridging chlorine as in **8**, relative to that of **1**$^{+\cdot}$ (analogues to **6**) by ca. 12 kcal mol^{-1}.[22] The inclusion of correlation energy will probably lower the relative energies of the bridged transition states further as found in comparing **8** with **6** (see above). Experience shows that geometry optimizations at the 4-31G or at higher levels should also lower the energy of the transition states relative to that of **1**$^{+\cdot}$. We therefore conclude that the experimental activation energy for the process **1**$^{+\cdot}$ → **8** + CO_2 is considerably lower than 45 kcal mol^{-1}, probably in the range 15–25 kcal mol^{-1}.

A direct consequence of Scheme I is that the formation of $CH_3ClCH_2^{+\cdot}$ and CO_2 from **1**$^{+\cdot}$ should be associated with a kinetic-energy release, T, as according to the calculation, there is a substantial reverse activation energy. A kinetic-energy release is indeed found experimentally. The kinetic-energy release, $T^{0.5}$, for CO_2 loss from **1**$^{+\cdot}$ corresponds to 0.62 kcal mol^{-1} (Gaussian signal), and the fact that CO_2 losses from **2**$^{+\cdot}$, **4**$^{+\cdot}$, and **5**$^{+\cdot}$ also give rise to Gaussian signals of $T^{0.5}$ = 0.71, 0.40, and 0.76 kcal mol^{-1}, respectively, may indicate qualitatively similar overall reaction profils.

Experimental Section

General Procedures. The collisional activation (CA) mass spectra were obtained with the use of a Varian MAT 311A double-focusing mass spectrometer in which ions pass through the magnetic field (B) before entering the electric field (E). The collision cell was differentially pumped and situated in front of the energy-resolving slit. Samples were introduced via the heated gas inlet system. The source temperature was 150–180 °C, the uncorrected ionizing energy of the electron beam 70 eV, and the accelerating voltage 3 kV. The magnetic and electric fields were adjusted to transmit exclusively the $C_2H_5X^{+\cdot}$ and $C_2H_4X_2^{+\cdot}$ ions. Helium was then introduced into the collision cell via a variable leak until the precursor ion abundance decreased to one-third of its original value due to scattering and decomposition. CA spectra were then obtained either by scanning the electrostatic sector potential (MIKES methodology[8]) or by a simultaneous scanning of the magnetic and electric fields (linked B/E scan[6]). The data were directly recorded on a XY recorder and normalized to the sum of the fragment ion intensities. Only peak heights were measured, and the abundances were not corrected for reduced multiplier response. The CA spectra are mean values of at least three (and at most five) measurements. The reproducibility was ±3–10% depending on the abundance of the precursors.

Materials. The methyl haloacetates **1**–**5** were prepared from the commercially available halo acid halides and methanol. For the preparation fo the methyl-d_3 esters (**1a**, **2a**) CD_3OD were used. CD_3CH_2Cl (**6a**) and CD_3CH_2Br (**7a**) were synthesized according to literature methods.[23] All compounds were characterized by ^{1}H NMR and purified by preparative gas chromatography.

Acknowledgment. Financial support of this work by the Deutsche Forschungsgemeinschaft (Project Schw 221/6-2), the Fonds der Chemischen Industrie, and the Technische Universität Berlin (Scientific Exchange Program, TU Berlin/Israel) and Dr. G. Bojesen's assistance in preparing the English version of this paper are gratefully acknowledged. We thank Prof. M. S. Gordon for a preprint of ref 13d, which includes the 6-31G* basis set for chlorine, and Dr. D. Cohen, Bar-Ilan University, for performing the UMP2/6-31G* calculations.

Registry No. **1**, 84893-52-7; **2**, 84836-48-6; **3**, 84836-49-7; **4**, 84836-50-0; **5**, 84836-51-1; **6**, 56339-90-3; **7**, 84893-53-8; **14**, 84848-86-2; **15**, 84836-54-4; **16**, 84836-55-5; **17**, 84848-87-3; **18**, 84836-56-6; 19, 84836-57-7; **20**, 24434-00-2; **8**, 84836-52-2; **10**, 84836-53-3; **11**, 557-91-5.

(21) See, for example: Hehre, W. J. In "Modern Theoretical Chemistry"; Schaefer, H. F., III, Ed.; Plenum Press: New York, 1977; Vol. 4.

(22) Unfortunately, 6-31G* calculations for the transition states could not be performed due to the large size of the systems. However, the 6-31G* and the UMP2/6-31G* calculations for **6** and **8** support this conclusion because they indicate that the 4-31G basis set underestimates the stability of chloronium-type structures (e.g., **8**) relative to regular alkyl chloride cation radicals. These results indicate that TS_1 and TS_2, which are of the chloronium type, are expected to be lowered in energy relative to TS_3 at 6-31G* and by correlation energy.

(23) (a) Pärkányi, C.; Sorm. F. *Collect. Czech. Chem. Commun.* **1963**, *28*, 2941. (b) Casey, C. D.; Cyr, C. R. *J. Am. Chem. Soc.* **1973**, *95*, 2248. (c) Lere-Porte, J. P.; Petrissans, J.; Gromb, S. *J. Mol. Struct.* **1976**, *34*, 55. (d) Benton, I. L.; Dillon, T. E. *J. Am. Chem. Soc.* **1942**, 64, 1128.